Coupled Systems Mechanics, *Vol. 6, No. 4 (2017) 501-522*
DOI: https://doi.org/10.12989/csm.2017.6.4.501

Iterative global-local approach to consider the local effects in dynamic analysis of beams

R. Emre Erkmen* and Ashkan Afnani[a]

School of Civil and Environmental Engineering, University of Technology, Sydney, 15 Broadway, Ultimo NSW 2007, Australia

(Received November 9, 2016, Revised November 13, 2017, Accepted November 14, 2017)

Abstract. This paper introduces a numerical procedure to incorporate elasto-plastic local deformation effects in the dynamic analysis of beams. The appealing feature is that simple beam type finite elements can be used for the global model which needs not to be altered by the localized elasto-plastic deformations. An overlapping local sophisticated 2D membrane model replaces the internal forces of the beam elements in the predefined region where the localized deformations take place. An iterative coupling technique is used to perform this replacement. Comparisons with full membrane analysis are provided in order to illustrate the accuracy and efficiency of the method developed herein. In this study, the membrane formulation is able to capture the elasto-plastic material behaviour based on the von Misses yield criterion and the associated flow rule for plane stress. The Newmark time integration method is adopted for the step-by-step dynamic analysis.

Keywords: iterative global-local method; multi-scale analysis; finite elements; elasto-plastic behavior; structural dynamics

1. Introduction

There is a need for computationally efficient structural dynamic analysis methods to gain savings in analysis time as well as in the post-processing of the results, despite significant advances in computer performances. It is possible to improve the accuracy of the numerical results by refining the model only in a local region without changing the global simpler model of the whole structure (Knight *et al.* 1991, Mao and Sun 1991, Mote 1971, Noor 1986). Simple beam elements are often used in the modelling of frame type structures, such as buildings or bridges, since frame-type structures are composed of beams and columns that have one dimension relatively large in comparison to the cross-sectional dimensions. Simple beam-type elements, however, are based on the assumption of rigid cross-section and thus, they cannot consider the deformations of the cross-section. On the other hand, local effects in beams may interact with the global behaviour to produce early yielding and reduction in strength. Overlapping decomposition

*Corresponding author, Ph.D., E-mail: emre.erkmen@uts.edu.au
[a]Ph.D., E-mail: ashkan.afnaniesfandabadi@student.uts.edu.au

http://www.techno-press.org/?journal=csm&subpage=8 ISSN: 2234-2184 (Print), 2234-2192 (Online)

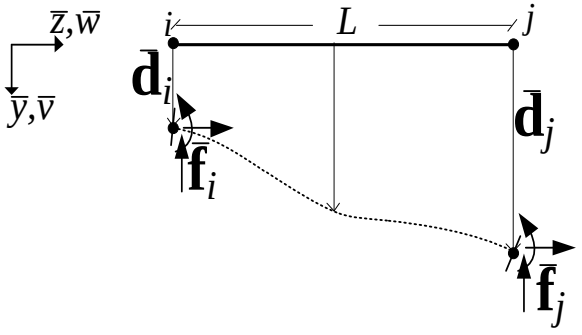

Fig. 1 Forces and displacements at the ends of the beam

2.1 Kinematic description

A beam element, based on the Euler-Bernoulli beam theory, is used for the global analysis of the structure. The formulation of this element is based on the three assumptions, which are: (a) beam axis stays perpendicular to the cross-section after deformations; (b) cross-sectional plane remains rigid throughout deformations; (c) normal stresses perpendicular to the axis line of the member are assumed to be zero. As shown in Fig. 1, vectors $\bar{\mathbf{d}}$ and $\bar{\mathbf{f}}$ are the end displacements and end forces of the beam before the local effects are considered. This initial configuration can be thought of as a trial state before the final configuration.

2.2 Strains

Strain components of the beam formulation can be written in terms of deflections $\bar{v}(\bar{z})$ and $\bar{w}(\bar{z})$, which are parallel to $\bar{y}$ and $\bar{z}$ directions, respectively as shown in Fig. 1. The generalized displacement field of a point on the cross-section is $\bar{\mathbf{u}} = \langle \bar{w}_p \quad \bar{v}_p \quad \bar{\theta}_p \rangle^{\mathrm{T}}$ where $\bar{\mathbf{u}} = \mathbf{N}\bar{\mathbf{d}}$, in which $\mathbf{N}$ is the matrix of interpolation functions and $\bar{\mathbf{d}}$ is the vector of nodal displacements. Matrix $\mathbf{N}$ can be written as $\mathbf{N} = \mathbf{YZ}$ in which

$$\mathbf{Z} = \begin{bmatrix} \mathbf{L}^{\mathrm{T}} & \mathbf{0} \\ \mathbf{0} & \mathbf{H}^{\mathrm{T}} \\ \mathbf{0} & \dfrac{\mathrm{d}\mathbf{H}^{\mathrm{T}}}{\mathrm{d}\bar{z}} \end{bmatrix}, \tag{1}$$

and

$$\mathbf{Y} = \begin{bmatrix} 1 & 0 & -\bar{y} \\ 0 & 1 & 0 \end{bmatrix}, \tag{2}$$

in which

$$\bar{\mathbf{E}} = \begin{bmatrix} E & 0 & 0 & 0 \\ 0 & 0 & 0 & 0 \\ 0 & 0 & 0 & 0 \\ 0 & 0 & 0 & 0 \end{bmatrix} \tag{10}$$

The variation of the strain field of a point on the cross-section of the beam element can also be decomposed into two parts which can be written as

$$\delta\bar{\boldsymbol{\varepsilon}} = \mathbf{S}\bar{\mathbf{B}}\delta\bar{\mathbf{d}}, \tag{11}$$

in which expressions $\bar{\mathbf{B}}$ can be written as $\bar{\mathbf{B}}=\nabla\mathbf{X}_a$ where

$$\nabla = \begin{bmatrix} \dfrac{\mathrm{d}}{\mathrm{d}z} & 0 \\ 0 & \dfrac{\mathrm{d}^2}{\mathrm{d}z^2} \end{bmatrix} \tag{12}$$

and

$$\mathbf{X}_a = \begin{bmatrix} \mathbf{L}^{\mathrm{T}} & \mathbf{0} \\ \mathbf{0} & \mathbf{H}^{\mathrm{T}} \end{bmatrix}. \tag{13}$$

By substituting Eq. (11) into Eq. (9), one obtains

$$\delta\bar{\Pi}=\delta\bar{\mathbf{d}}^{\mathbf{T}}\int_L\int_A \bar{\mathbf{B}}^{\mathrm{T}}\mathbf{S}^{\mathrm{T}}\bar{\boldsymbol{\sigma}}\mathrm{d}A\,\mathrm{d}\bar{z} + \delta\bar{\mathbf{d}}^{\mathbf{T}}\int_L\int_A \mathbf{N}^{\mathbf{T}}\mathbf{c}\dot{\bar{\mathbf{u}}}\mathrm{d}A\mathrm{d}\bar{z} + \delta\bar{\mathbf{d}}^{\mathbf{T}}\int_L\int_A \mathbf{N}^{\mathbf{T}}\boldsymbol{\rho}\ddot{\bar{\mathbf{u}}}\mathrm{d}A\mathrm{d}\bar{z} - \delta\bar{\mathbf{d}}^{\mathbf{T}}\bar{\mathbf{f}} = 0. \tag{14}$$

2.4 Linearization of the dynamic equilibrium equations

The incremental equilibrium equations can be obtained by subtracting the virtual work expressions in Eq. (14) at two neighbouring equilibrium states and then linearizing the result by omitting the second- and higher-order terms, i.e.,

$$\delta\left(\delta\bar{\Pi}\right)\approx \delta\bar{\mathbf{d}}^{\mathbf{T}}\bar{\mathbf{K}}\delta\bar{\mathbf{d}} + \delta\bar{\mathbf{d}}^{\mathbf{T}}\bar{\mathbf{C}}\delta\dot{\bar{\mathbf{d}}} + \delta\bar{\mathbf{d}}^{\mathbf{T}}\bar{\mathbf{M}}\delta\ddot{\bar{\mathbf{d}}} - \delta\bar{\mathbf{d}}^{\mathbf{T}}\delta\bar{\mathbf{f}} = 0, \tag{15}$$

where

$$\bar{\mathbf{K}} = \int_L\int_A \bar{\mathbf{B}}^{\mathrm{T}}\mathbf{S}^{\mathrm{T}}\bar{\mathbf{E}}\mathbf{S}\bar{\mathbf{B}}\mathrm{d}A\mathrm{d}\bar{z}, \tag{16}$$

$$\bar{\mathbf{C}} = \int_L\int_A \mathbf{N}^{\mathbf{T}}\mathbf{c}\mathbf{N}\mathrm{d}A\,\mathrm{d}\bar{z} \tag{17}$$

and

$$\hat{\mathbf{K}}=\int_L\int_A \hat{\mathbf{B}}^T\hat{\mathbf{C}}_{ep}\hat{\mathbf{B}}\,dA\,d\bar{z}\,, \tag{22}$$

where $\hat{\mathbf{C}}_{ep}$ is the elasto-plastic stress-strain matrix as explained in section 4.1. and

$$\hat{\mathbf{C}}=\int_L\int_A \hat{\mathbf{X}}^T\mathbf{c}\hat{\mathbf{X}}\,dA\,d\bar{z} \tag{23}$$

$$\hat{\mathbf{M}}=\int_L\int_A \hat{\mathbf{X}}^T\boldsymbol{\rho}\hat{\mathbf{X}}\,dA\,d\bar{z} \tag{24}$$

where $\delta\hat{\mathbf{u}}=\hat{\mathbf{X}}\delta\hat{\mathbf{d}}$ was used.

3.2 Displacement decomposition

The membrane displacement vector is decomposed into two parts: a global component, which is in accordance with the kinematic assumption of the beam element, and a remaining part that is the difference between the total membrane displacements and the global component. To build the global component, a decomposition operator is adopted that projects the nodal displacement of the beam onto the nodal points of the membrane model, i.e., $\hat{\mathbf{d}}=\mathbf{N}\bar{\mathbf{d}}+\mathbf{d}'$, the variation of the membrane nodal displacement vector can be written as

$$\delta\hat{\mathbf{d}}=\mathbf{N}\delta\bar{\mathbf{d}}+\delta\mathbf{d}', \tag{25}$$

It should be noted that as opposed to its use in section 2.1, where it was imposing the kinematic conditions on a continuum, $\mathbf{N}$ operates on discrete coordinates $\bar{y}$ and $\bar{z}$ of the local membrane model nodes. By adopting $\mathbf{N}$ as the decomposition operator, it is assumed that outside of the overlapping region where $\mathbf{d}'$ is a zero vector, the beam displacements are identical with those of the possible membrane solution.

3.3 Coupled global and local equilibrium equations

We can decompose the first variation of the membrane strain based on the abovementioned decomposition of the variation of the displacement vector $\delta\hat{\mathbf{d}}$ by substituting Eq. (25) into Eq. (20), i.e., $\delta\hat{\boldsymbol{\varepsilon}}=\delta\bar{\boldsymbol{\varepsilon}}+\delta\boldsymbol{\varepsilon}'$, where

$$\delta\bar{\boldsymbol{\varepsilon}}=\hat{\mathbf{B}}\mathbf{N}\delta\bar{\mathbf{d}}\,, \tag{26}$$

and

$$\delta\boldsymbol{\varepsilon}'=\hat{\mathbf{B}}\delta\mathbf{d}'\,. \tag{27}$$

As discussed previously, the first component of the membrane displacement is obtained by imposing beam kinematics on the membrane solution. Consequently, the variation of this component of the membrane strain vector is equal to that of the beam i.e., $\hat{\mathbf{B}}\mathbf{N}=\mathbf{S}\bar{\mathbf{B}}$. The second

be written as

$$\delta\mathbf{c} = -\left[\mathbf{N}^{\mathrm{T}}\hat{\mathbf{K}}\mathbf{N}\right]^{-1}\left[\mathbf{N}^{\mathrm{T}}\int_{L}\int_{A}\hat{\mathbf{B}}^{\mathrm{T}}\left(\hat{\mathbf{C}}_{ep}-\bar{\mathbf{E}}\right)\hat{\mathbf{B}}\mathrm{d}A\mathrm{d}z\mathbf{N}-\bar{\mathbf{K}}\right]\delta\bar{\mathbf{d}}\,, \tag{34}$$

It should also be noted that matrices $\mathbf{Q}_{\mathbf{C}}$ and $\mathbf{Q}_{\mathbf{M}}$ can be selected as

$$\mathbf{Q}_{\mathbf{C}}=\boldsymbol{\Omega}_{\mathbf{C}}-\mathbf{N}\left[\mathbf{N}^{\mathrm{T}}\hat{\mathbf{C}}\mathbf{N}\right]^{-1}\mathbf{N}^{\mathrm{T}}\hat{\mathbf{C}}\boldsymbol{\Omega}_{\mathbf{C}}\,, \tag{35}$$

and

$$\mathbf{Q}_{\mathbf{M}}=\boldsymbol{\Omega}_{\mathbf{M}}-\mathbf{N}\left[\mathbf{N}^{\mathrm{T}}\hat{\mathbf{M}}\mathbf{N}\right]^{-1}\mathbf{N}^{\mathrm{T}}\hat{\mathbf{M}}\boldsymbol{\Omega}_{\mathbf{M}}\,, \tag{36}$$

where $\boldsymbol{\Omega}_{\mathbf{K}}$, $\boldsymbol{\Omega}_{\mathbf{C}}$ and $\boldsymbol{\Omega}_{\mathbf{M}}$ are time dependent matrix functions to build the relations $\delta\ddot{\mathbf{d}}'=\partial\left(\delta\dot{\mathbf{d}}'\right)/\partial t=\partial^2\left(\delta\mathbf{d}'\right)/\partial t^2$.

By linearization of Eq. (29) we have;

$$\delta\left(\delta\Pi_2\right)\approx\delta\mathbf{d}'^{\mathrm{T}}\hat{\mathbf{K}}\delta\hat{\mathbf{d}}-\delta\mathbf{d}'^{\mathrm{T}}\delta\hat{\mathbf{f}}=0\,. \tag{37}$$

It should be noted that the difference between Eqs. (21) and (37) is due to multiplication of the equations with $\delta\mathbf{d}'^{\mathbf{T}}$ instead of $\delta\hat{\mathbf{d}}^{\mathbf{T}}$. Considering the arbitrariness of both vectors, it can be concluded that both Eqs. (21) and (37) admit the same solution, which is the result of the membrane analysis for the whole domain of the structure. However, the solution of the beam model is deemed sufficiently accurate in regions that are not in the proximity of the localized behaviour where the local membrane solution is avoided for economy.

3.5 Interface boundary conditions

We obtain the local membrane solution within the overlapping domain by using the beam element displacement values as boundary conditions for the membrane model. It should be noted that the displacements of a point at the interface can be calculated only from the beam nodal displacements, i.e., $\mathbf{N}_{@i\&j}\bar{\mathbf{d}}$. Subscript $i\,\&\,j$ indicate both ends of the local membrane model. One important issue to be addressed before imposing the membrane boundary conditions is that even if there are no local effects, Poisson ratio effect causes change in the cross-sectional dimensions throughout the analysis domain. However, beam analysis does not produce a displacement field within the plane of the cross-section that captures the changes in cross-sectional dimensions due to Poisson ratio effect. On the other hand, this effect is considered in the stress field by adopting a separate constitutive relation in the beam formulation. Indeed, within the analysis region where beam solution is deemed accurate, we implicitly impose a strain field which can be considered within the current analysis framework as the Poisson ratio effect in the beam solution, i.e., $\boldsymbol{\varepsilon}'=\begin{pmatrix}0 & -\nu\varepsilon & 0 & 0\end{pmatrix}^{\mathrm{T}}$, in which ε indicates the axial strain. It is important to note that this Poisson ratio effect has no influence on the beam equilibrium equations and the nodal displacement vector, because the associated stress field is a zero vector, i.e., $\boldsymbol{\sigma}'=\begin{pmatrix}0 & 0 & 0 & 0\end{pmatrix}^{\mathrm{T}}$.

the hardening modulus and λ is the effective plastic strain. If the trial stress $\hat{\boldsymbol{\sigma}}^{tr}$ is outside the yield surface the Closest-Point Projection algorithm as given in Simo and Hughes (1998) is adopted to impose the flow rule and the consistency condition.

4.1 Elasto-plastic constitutive equations and stress update

The vector of stresses can be written as

$$\hat{\boldsymbol{\sigma}} = \left\langle \hat{\sigma}_x \quad \hat{\sigma}_y \quad \hat{\tau}_{xy} \mid \hat{\tau}_m \right\rangle^{\mathrm{T}}. \tag{39}$$

and the matrix of elastic material properties of the membrane element $\hat{\mathbf{E}}$ can be written as

$$\hat{\mathbf{E}} = \frac{E}{\left(1-\nu^2\right)} \left[\begin{array}{ccc:c} 1 & \nu & 0 & 0 \\ \nu & 1 & 0 & 0 \\ 0 & 0 & \dfrac{1-\nu}{2} & 0 \\ \hdashline 0 & 0 & 0 & \dfrac{(1-\nu)}{2} \end{array}\right] \tag{40}$$

in which E is the Young's modulus and ν is the Poisson's ratio. It should be noted that the last diagonal term in Eq. (40) is because of the modification introduced into the potential energy functional. The continuum elasto-plastic stress-strain relations can be written as

$$\mathrm{d}\hat{\boldsymbol{\sigma}} = \hat{\mathbf{E}}\mathrm{d}\hat{\boldsymbol{\varepsilon}} - \mathrm{d}\lambda\hat{\mathbf{E}}\mathbf{a} \tag{41}$$

in which $\mathbf{a}=\partial f / \partial \hat{\boldsymbol{\sigma}}$. The consistency condition during plastic deformation, i.e., $\mathrm{d}f = 0$ and $\mathrm{d}\hat{\boldsymbol{\sigma}} = \hat{\mathbf{E}}\left(\mathrm{d}\hat{\boldsymbol{\varepsilon}} - \mathrm{d}\lambda\mathbf{a}\right)$ produces $\mathrm{d}\lambda = \mathbf{a}^{\mathrm{T}}\hat{\mathbf{E}}\mathrm{d}\hat{\boldsymbol{\varepsilon}} \big/ \left(\mathbf{a}^{\mathrm{T}}\hat{\mathbf{E}}\mathbf{a} + H\right)$. After yielding occurs, the flow rule and the consistency condition can be imposed in an incremental iterative procedure. Respectively, the flow rule and the consistency condition can be written in finite incremental form as

$$\mathbf{r} = \Delta\hat{\boldsymbol{\sigma}} - \hat{\mathbf{E}}\Delta\hat{\boldsymbol{\varepsilon}} + \Delta\lambda\hat{\mathbf{E}}\mathbf{a} = 0 \tag{42}$$

$$f\left(\hat{\boldsymbol{\sigma}}\right) = 0 \tag{43}$$

The nonlinear set of Eqs. (42) and (43) can be solved according to the Newton-Raphson solution scheme as

$$\begin{bmatrix} \mathbf{I} + \Delta\lambda\hat{\mathbf{E}}\nabla^2 f & \hat{\mathbf{E}}\mathbf{a} \\ \mathbf{a}^{\mathrm{T}} & -H \end{bmatrix} \begin{Bmatrix} \delta\hat{\boldsymbol{\sigma}} \\ \delta\lambda \end{Bmatrix}^{j} = -\begin{Bmatrix} \mathbf{r} \\ f \end{Bmatrix}^{j} \tag{44}$$

$$\Delta\bar{\mathbf{R}}_k^n=\bar{\mathbf{f}}_k-\mathbf{N}^{\mathrm{T}}\int_L\int_A\hat{\mathbf{B}}_k^{n\mathrm{T}}\hat{\mathbf{S}}^{\mathrm{T}}\hat{\boldsymbol{\sigma}}_k^n\mathrm{d}A\mathrm{d}z-\mathbf{N}^{\mathrm{T}}\hat{\mathbf{C}}\dot{\hat{\mathbf{d}}}_k^n-\mathbf{N}^{\mathrm{T}}\hat{\mathbf{M}}\ddot{\hat{\mathbf{d}}}_k^n \tag{50}$$

The incremental displacement vector $\Delta\bar{\mathbf{d}}_k^n$ can be used to update the displacement $\bar{\mathbf{d}}_k^n=\bar{\mathbf{d}}_k^{n-1}+\Delta\bar{\mathbf{d}}_k^n$, velocity $\dot{\bar{\mathbf{d}}}_k^n=\dot{\bar{\mathbf{d}}}_k^{n-1}+\Delta\dot{\bar{\mathbf{d}}}_k^n$ and acceleration $\ddot{\bar{\mathbf{d}}}_k^n=\ddot{\bar{\mathbf{d}}}_k^{n-1}+\Delta\ddot{\bar{\mathbf{d}}}_k^n$ vectors of the global solution in each iteration *n*, where

$$\Delta\ddot{\bar{\mathbf{d}}}_k^n=\frac{4}{\delta t^2}\Delta\bar{\mathbf{d}}_k^n-\delta\frac{4}{\delta t}\dot{\bar{\mathbf{d}}}_k^{n-1}-2\ddot{\bar{\mathbf{d}}}_k^{n-1}, \tag{51}$$

and

$$\Delta\dot{\bar{\mathbf{d}}}_k^n=\frac{2}{\delta t}\Delta\bar{\mathbf{d}}_k^n-2\dot{\bar{\mathbf{d}}}_k^{n-1}, \tag{52}$$

have been used based on Newmark's constant acceleration method. For the current time $t+\Delta t$, local, displacements and stresses used in Eq. (50) can be updated using the local model in an incremental-iterative manner; firstly, displacement, velocity and acceleration boundary conditions and the load within the global step *k*, are increasingly imposed in *s* steps and; secondly, the displacement increments of the internal nodes are determined in *l* iterations, i.e., $\Delta\hat{\mathbf{d}}_{IN\,s}^{\,l}$, because the unbalanced terms due nonlinearities in the local model, i.e., $\Delta\hat{\mathbf{r}}_{IN\,s}^{\,l}$ should also be corrected in the local model. Thus, from Eq. (38), by using the Newmark's constant acceleration procedure, the local displacement vector of the internal nodes at the l^{th} iteration $\Delta\hat{\mathbf{d}}_{IN\,s}^{\,l}$ can be written as

$$\Delta\hat{\mathbf{d}}_{IN\,s}^{\,l}=\breve{\mathbf{K}}_{c\,s}^{-1}\left(\Delta\breve{\mathbf{f}}_{I\,s}+\Delta\hat{\mathbf{r}}_{IN\,s}^{\,l}-\hat{\mathbf{K}}_b^{\mathrm{T}}{}_s\Delta\hat{\mathbf{d}}_{s\,@i\&j}-\hat{\mathbf{C}}_b^{\mathrm{T}}\Delta\dot{\hat{\mathbf{d}}}_{s\,@i\&j}-\hat{\mathbf{M}}_b^{\mathrm{T}}\Delta\ddot{\hat{\mathbf{d}}}_{s\,@i\&j}\right) \tag{53}$$

in which $\breve{\mathbf{K}}_{c\,s}$ is due to partitioning of the effective stiffness matrix of the local membrane model which is updated in each step *s*, i.e.,

$$\breve{\mathbf{K}}_{c\,s}=\hat{\mathbf{K}}_{c\,s}+\frac{2}{\Delta t_s}\hat{\mathbf{C}}_c+\frac{4}{\Delta t_s^{\,2}}\hat{\mathbf{M}}_c \tag{54}$$

and $\Delta\breve{\mathbf{f}}_{I\,s}$ is the due to the portioning of the effective load vector in step *s*, i.e.,

$$\Delta\breve{\mathbf{f}}_{I\,s}=\Delta\hat{\mathbf{f}}_{I\,s}+\hat{\mathbf{M}}_c\left(\frac{4}{\Delta t_s}\dot{\hat{\mathbf{d}}}_{IN\,s}^{\,l}+2\ddot{\hat{\mathbf{d}}}_{IN\,s}^{\,l}\right)+2\hat{\mathbf{C}}\dot{\hat{\mathbf{d}}}_{IN\,s}^{\,l}. \tag{55}$$

The incremental displacement vector $\Delta\hat{\mathbf{d}}_{IN\,s}^{\,l}$ can be used to update the displacement $\hat{\mathbf{d}}_{IN\,s}^{\,l}=\hat{\mathbf{d}}_{IN\,s}^{\,l-1}+\Delta\hat{\mathbf{d}}_{IN\,s}^{\,l}$, velocity $\dot{\hat{\mathbf{d}}}_{IN\,s}^{\,l}=\dot{\hat{\mathbf{d}}}_{IN\,s}^{\,l-1}+\Delta\dot{\hat{\mathbf{d}}}_{IN\,s}^{\,l}$ and acceleration $\ddot{\hat{\mathbf{d}}}_{IN\,s}^{\,l}=\ddot{\hat{\mathbf{d}}}_{IN\,s}^{\,l-1}+\Delta\ddot{\hat{\mathbf{d}}}_{IN\,s}^{\,l}$ vectors of the local solution in each iteration *n*. It should be noted that the time step Δt_s is in general different from that of the global step, i.e., $\Delta t_s=\Delta t/s$ if the dynamic solution of the local membrane model

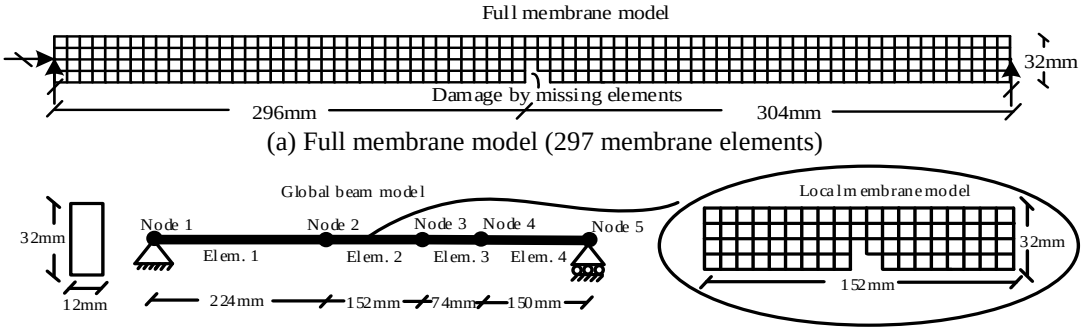

(a) Full membrane model (297 membrane elements)

(b) Global-local model (73 membrane elements)

Fig. 2 Model dimensions and boundary conditions in Examples 1 and 2

In both axial and vertical loading cases, the results of the global-local analysis are compared with those of the full membrane analysis for verification purposes as shown in Figs. 3-6. In order to be able to impose the same boundary and loading conditions for membrane and the global-local model throughout the analysis, warping of the cross-section at the ends due to applied loads are prevented by applying Multiple-point constraints at the ends of the membrane model. It should be noted that the same 10^{-5} error tolerance in the Euclid norm of the force vectors is used for convergence check, and the damping constant c is selected as 5×10^{-5} in all cases.

Initially a compressive impact load is applied at the tip (Node 5) of the beam as shown in Fig. 3, and the tip displacement vs. time behaviour is plotted.

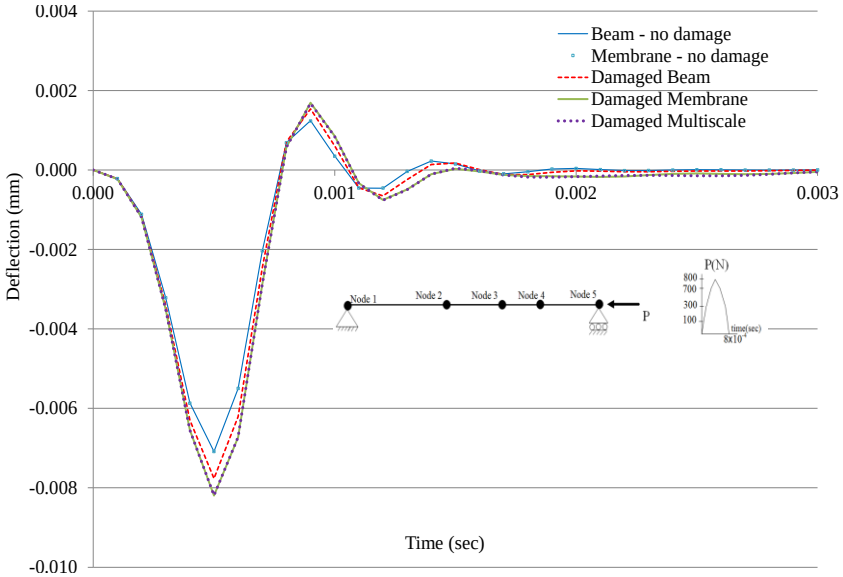

Fig. 3 Axial deflection at the tip vs. time

As shown in Fig. 3, the beam and the membrane solutions fully agree when there is no damage

damage introduced (i.e., full 300 element membrane model is used) thus, beam solution is very economical. However, when damage is introduced by removing 3 elements at the mid-span of the beam the membrane solution and the beam solution do not agree. On the other hand, the global-local analysis is in excellent agreement with the full membrane analysis as shown in Fig. 5 as well as Fig. 6 where the frequency response functions of the displacements are plotted based on the Fast Fourier Transform of the data.

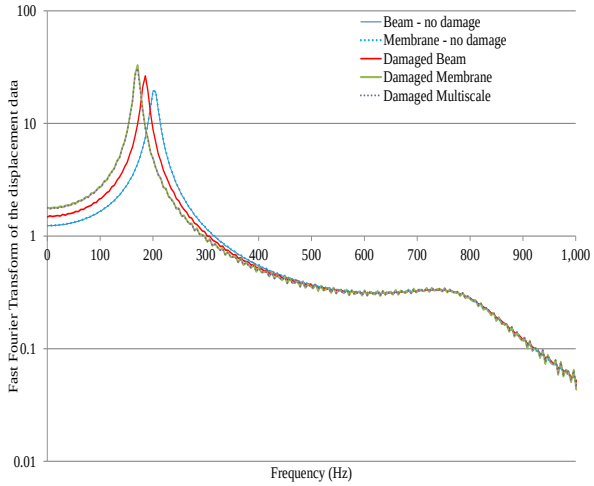

Fig. 6 Fast Fourier Transform of the vertical deflection at Node 4

6.2 Elasto-plastic dynamic analysis of a steel plate shear wall with opening

A cantilever steel plate shear wall with an opening at its base subjected to a cyclic load of $P = 250\times10^{3}\times\sin\left(2\pi\times100t\right)$ N at its tip is analysed in this section (Fig. 7).

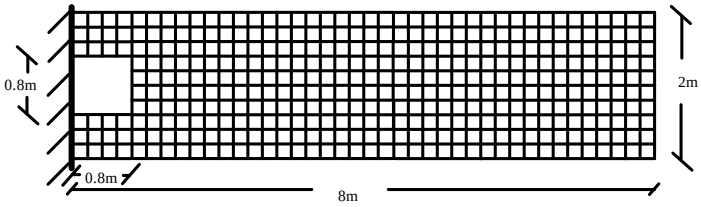

(a) Full membrane model (384 membrane elements)

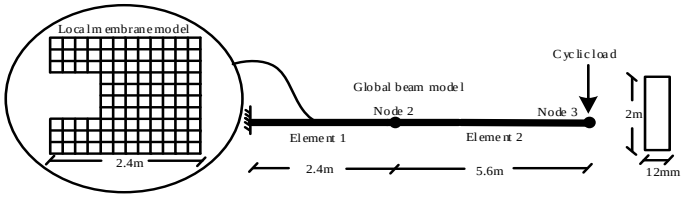

(b) Global-local model (104 membrane elements)

Fig. 7 Model dimensions and boundary conditions in Example 3

7. Conclusions

An iterative global-local method is developed in this study to consider the local effects in the global dynamic behavior of beams. The method implements an overlapping domain decomposition technique to allow the use of beam elements for the global model while adopting sophisticated elasto-plastic membrane elements in the regions where localized deformations are anticipated. Several cases are studied using the developed method and excellent agreement with the full membrane solution is observed. By adopting the proposed method, significant reduction in the number of degrees-of-freedom of the finite element model can be achieved without noticeable compromise in the accuracy of the analysis, which signifies the efficiency of the method in the dynamic analysis of structures with localized nonlinearities.

References

Allix, O., Gendre, L., Gosselet, P. and Guguin, G. (2011), "Non-intrusive coupling: An attempt to merge industrial and research software capabilities", *Rec. Develop. Innovat. Appl. Comput. Mech.*, **15**, 125-133.

Afnani, A. and Erkmen, R.E. (2016)**,** "Iterative global-local procedure for the analysis of composite thin-walled laminates", *Steel Compos. Struct.*, **20**, 693-718.

Babuska, I. and Melenk, J.M. (1995), *The Partition of Unity Finite Element Method (Final Report, Apr. - Jun. 1995)*, Vol. AD-A301760, TN-BN-1185, NIPS-96-41139.

Banik, S.S., Hong, H.P. and Kopp G.A. (2010), "Assesment of capcity curves for tranmission line towers under wind loading", *Wind Struct.*, **13**(1), 1-20.

Belytschko, T. (2001), "Arbitrary discontinuities in finite elements", *J. Numer. Meth. Eng.*, **50**(4), 993-1013.

Belytschko, T., Krongauz, Y., Organ, D., Fleming, M. and Krysl, P. (1996), "Meshless methods: An overview and recent developments", *Comput. Meth. Appl. Mech. Eng.*, **139**(1), 3-47.

Bettinotti, O., Allix, O. and Malherbe, B. (2014), "A coupling strategy for adaptive local refinement in space time with a fixed global model in explicit dynamics", *Comput. Mech.*, **53**, 561-574.

Bozdogan, K.B. and Ozturk, D. (2016), "A method for dynamic analysis of frame-hinged shear wall structures", *Earthq. Struct.*, **11**(1), 45-61.

Doyle, J.F. and Farris, T.N. (1995), "Structural mechanics modeling of the impact of a double cantilever beam", *J. Fract.*, **76**(4), 311-326.

Duarte, C. and Oden, J. (1996), "Hp clouds-an hp meshless method", *Numer. Meth. Part. Differ. Equat.*, **12**, 673-705.

Duval, M., Passieux, J.C., Salaün, M. and Guinard, S. (2016), "Non-intrusive coupling: Recent advances and scalable nonlinear domain decomposition", *Arch. Comput. Meth. Eng.*, **23**(1), 17-38.

Erkmen, E. and Bradford, M.A. (2011), "Coupling of finite element and meshfree methods for locking-free analysis of shear-deformable beams and plates", *Eng. Comput.*, **28**(8), 1003-27.

Erkmen, R. (2013), "Bridging multi-scale approach to consider the effects of local deformations in the analysis of thin-walled members", *Comput. Mech.*, **52**(1), 65-79.

Erkmen, R.E. (2015), "Multiple-point constraint applications for the finite element analysis of shear deformable composite beams-variational multiscale approach to enforce full composite action", *Comput. Struct.*, **149**, 17-30.

Erkmen, R.E., Saleh, A. and Afnani, A. (2016), "Incorporating local effects in the predictor step of the iterative global-local analysis of beams", *J. Multisc. Comput. Eng.*, **14**, 455-477.

Erkmen, R.E. and Saleh, A. (2017), "Iterative global-local approach to consider the effects of local elasto-plastic deformations in the analysis of thin-walled members", *J. Multisc. Comput. Eng.*, **15**, 143-173.

Erkmen, R.E., Mohareb, M. and Afnani, A. (2017), "Multi-scale overlapping domain decomposition to consider elasto-plastic local buckling effects in the analysis of pipes", *J. Struct. Stab. Dyn.*, **17**, 1-28.

Appendix

A.1 Interpolation functions of the membrane

The vector of the displacement field shown in Fig. 1(b) can be written as

$$\hat{\mathbf{u}} = \left\langle \hat{u}_0 \quad \hat{v}_0 \quad \hat{\theta} \right\rangle^{\mathrm{T}} \tag{A. (1)}$$

which can be interpolated by using nodal displacements as

$$\hat{\mathbf{u}} = \hat{\mathbf{X}}\hat{\mathbf{d}}\,, \tag{A. (2)}$$

where the nodal displacement vector of an element can be written as

$$\hat{\mathbf{d}} = \left\langle \hat{u}_1 \quad \hat{v}_1 \quad \hat{\theta}_1 \quad \hat{u}_2 \quad \hat{v}_2 \quad \hat{\theta}_2 \quad \hat{u}_3 \quad \hat{v}_3 \quad \hat{\theta}_3 \quad \hat{u}_4 \quad \hat{v}_4 \quad \hat{\theta}_4 \right\rangle^{\mathrm{T}}, \tag{A. (3)}$$

and matrix $\hat{\mathbf{X}}$ in Eq. A. (2) can be written as

$$\hat{\mathbf{X}} = \left[\begin{array}{ccc:ccc:ccc:ccc} N_1 & 0 & N_1^x & N_2 & 0 & N_2^x & N_3 & 0 & N_3^x & N_4 & 0 & N_4^x \\ 0 & N_1 & N_1^y & 0 & N_2 & N_2^y & 0 & N_3 & N_3^y & 0 & N_4 & N_4^y \\ 0 & 0 & N_1 & 0 & 0 & N_2 & 0 & 0 & N_3 & 0 & 0 & N_4 \end{array}\right] \tag{A. (4)}$$

in which N_i is the standard bilinear shape function defined as

$$N_i = \frac{1}{4}\left(1+\xi_i\xi\right)\left(1+\eta_i\eta\right),\ i = 1,2,3,4 \tag{A. (5)}$$

where $\xi = x/a$ and $\eta = y/b$, a and b are the half lengths of the rectangular member in x and y directions respectively. Local coordinates x and y are measured from the middle of the rectangular element, i.e., $-1 \le \xi \le 1$ and $-1 \le \eta \le 1$. It should also be noted that 2×2 Gaussian quadrature was used for the numerical integration of both plate and membrane. Membrane related functions N_i^x and N_i^y according to Allman-type interpolation are defined as

$$N_i^x = \frac{1}{8}\left(y_{ij}N_l - y_{ik}N_m\right),\ (i = 1,2,3,4) \tag{A. (6)}$$

$$N_i^y = \frac{1}{8}\left(x_{ij}N_l - x_{ik}N_m\right),\ (i = 1,2,3,4) \tag{A. (7)}$$

in which

$$N_m = \frac{1}{2}\left(1-\xi^2\right)\left(1+\eta_m\eta\right),\ (m = 8,5,6,7) \tag{A. (8)}$$

$$N_l = \frac{1}{2}\left(1+\xi_l\xi\right)\left(1-\eta^2\right), (l=5,6,7,8). \quad \text{A. (9)}$$

where $x_{ij}=x_j-x_i$, $y_{ij}=y_j-y_i$, ${l_{ij}}^2={x_{ij}}^2+{y_{ij}}^2$, $(ij=41,12,23,34)$ and $(ik=12,23,34,41)$.

A.2 Strains of the membrane element

Strains of the membrane element can be written as

$$\hat{\boldsymbol{\varepsilon}} = \left\langle \hat{\varepsilon}_x \quad \hat{\varepsilon}_y \quad \hat{\gamma}_{xy} \;\vdots\; \hat{\gamma}_m \right\rangle^{\mathrm{T}} \quad \text{A. (10)}$$

where

$$\hat{\boldsymbol{\varepsilon}} = \left\langle \frac{\partial \hat{u}_0}{\partial x} \quad \frac{\partial \hat{v}_0}{\partial y} \quad \frac{\partial \hat{u}_0}{\partial y}+\frac{\partial \hat{v}_0}{\partial x} \;\vdots\; \frac{1}{2}\left(\frac{\partial \hat{v}_0}{\partial x}-\frac{\partial \hat{u}_0}{\partial y}\right)-\hat{\theta} \right\rangle^{\mathrm{T}} = \left\{ \begin{array}{c} \hat{\boldsymbol{\varepsilon}}_m \\ \hline \frac{1}{2}\left(\frac{\partial \hat{v}_0}{\partial x}-\frac{\partial \hat{u}_0}{\partial y}\right)-\hat{\theta} \end{array} \right\}, \quad \text{A. (11)}$$

in which $\hat{\boldsymbol{\varepsilon}}_m$ is the vector of membrane strains and the last row in Eq. A. (11) contains the skew symmetric part of the membrane strains introduced to avoid numerical stability issues when drilling rotations $\hat{\theta}$ are used with Allman-type interpolations [27].

Matrix $\hat{\mathbf{B}}$ can be written as

$$\hat{\mathbf{B}} = \bar{\mathbf{B}}_m \Im \hat{\mathbf{X}} \quad \text{A. (12)}$$

in which

$$\bar{\mathbf{B}}_m = \begin{bmatrix} 1 & 0 & 0 & 0 & 0 \\ 0 & 1 & 0 & 0 & 0 \\ 0 & 0 & 1 & 1 & 0 \\ 0 & 0 & -\frac{1}{2} & \frac{1}{2} & -1 \end{bmatrix}, \quad \text{A. (13)}$$

$$\Im = \begin{bmatrix} \frac{\partial}{\partial x} & 0 & \frac{\partial}{\partial y} & 0 & 0 \\ 0 & \frac{\partial}{\partial y} & 0 & \frac{\partial}{\partial x} & 0 \\ 0 & 0 & 0 & 0 & 1 \end{bmatrix}^{\mathrm{T}}, \quad \text{A. (14)}$$